Breaking the PFAS Chain: Piezocatalytic Decomposition of Forever Chemicals Using BaTiO₃ Nanoparticles

Andrea Veciana, Sarah Steiner, Qiao Tang, Vitaly Pustovalov, Joaquim Llacer, Jiang Wu, Xiang-Zhong Chen, Trust Manyiwa, Venecio U. Ultra Jr., Beltzane Garcia-Cirera, Josep Puigmartí-Luis, Carlos Franco, David J. Janssen, Laura Nyström, Samy Boulos*, Salvador Pané*

A. Veciana, S. Steiner, Q. Tang, V. Pustovalov, J. Wu, C. Franco, S. Pané
Institute of Robotics and Intelligent Systems ETH Zurich, Tannenstrasse 3, Zurich CH 8092, Switzerland

David J. Janssen
Eawag: Swiss Federal Institute of Aquatic Science & Technology, Department Surface Waters, 6047 Kastanienbaum, Switzerland

Trust Manyiwa, Venecio U. Ultra Jr.,
Department of Earth & Environmental Science, Faculty of Science, Botswana International University of Science and Technology, Palapye, Botswana

L. Nyström, S. Boulos
Laboratory of Food Biochemistry, Department of Health Sciences and Technology, ETH Zurich, Schmelzbergstrasse 9, 8092 Zürich, Switzerland.

X.-Z. Chen
Institute of Optoelectronics, State Key Laboratory of Photovoltaic Science and Technology, Shanghai Frontiers Science Research Base of Intelligent Optoelectronics and Perception, International Institute of Intelligent Nanorobots and Nanosystems, Fudan University, Shanghai 200433, People's Republic of China
Yiwu Research Institute of Fudan University
Yiwu, Zhejiang 322000, People's Republic of China

Josep Puigmartí-Luis[1,2], Beltzane Garcia-Cirera[1]
[1]Departament de Ciència de Materials i Química Física, Institut de Química Teòrica i Computacional, Universitat de Barcelona, Barcelona 08028, Spain
[2]Institució Catalana de Recerca i Estudis Avançats (ICREA)
Pg. Lluís Companys 23, Barcelona 08010, Spain

1

Per- and polyfluoroalkyl substances (PFAS) pose significant environmental and health risks due to their ubiquitous presence and persistence in water systems. In this study, we investigate the efficacy of piezocatalysis using barium titanate (BTO) nanoparticles under ultrasound irradiation for the degradation and defluorination of perfluorooctane sulfonate (PFOS) in water. The research demonstrates a substantial 90.5% degradation and 29% defluorination of PFOS after six hours of treatment, highlighting the potential of piezocatalysis as a promising approach for PFAS degradation. Additionally, the quantification of degradation products elucidates the transformation pathways of PFOS, suggesting a stepwise chain-shortening mechanism. Our findings underscore the importance of continued research in optimizing piezocatalytic processes and exploring synergistic approaches with other advanced oxidation methods to effectively address PFAS contamination challenges. These efforts are essential for advancing sustainable water treatment strategies and mitigating the environmental and health hazards associated with PFAS contamination.

1. Introduction

Per- and polyfluoroalkyl substances (PFAS) represent a group of synthetic chemicals employed in various industrial and consumer products for decades. Known for their thermal and chemical stability, PFAS are denoted as 'forever chemicals' for their enduring presence in the environment [1]. PFAS are characterized by a hydrophobic fluorinated carbon chain linked to a hydrophilic functional group, as depicted in **Figure 1**. Their highly stable C–F bond provides PFAS a superior chemical stability, making them instrumental in several applications, including non-stick cookware, water repellent fabrics, and firefighting foams [2, 3]. However, growing environmental concerns have prompted stringent regulations, including the restriction of production and use of PFAS such as perfluorooctanoic acid (PFOA) and perfluorooctane sulfonate (PFOS) under the 2009 Stockholm Convention [4]. In 2019, the convention imposed a general ban on the production of PFOA and its precursors.

Despite regulatory efforts, the widespread use of PFAS has resulted in their release into the environment, where they can persist for many years and spread over long distances [3, 5]. PFAS have been detected in soil, water, wildlife, and human blood and tissues [6, 7]. In Switzerland, where 80% of drinking water originates from groundwater, National Groundwater Monitoring NAQUA reveals that the sum of 26 PFAS species present in ground water exceed the established limits proposed by the European Commission of 0.0044 µg L^{-1} on 25% of the monitoring sites [8]. Moreover, the potential health risks associated with PFAS contamination, such as increased cancer risks, thyroid dysfunction, and reproductive disorders, further emphasize the urgency of establishing robust and comprehensive water treatment strategies to safeguard both environmental ecosystems and human health [9-11].

As a result, there has been a growing effort to regulate PFAS and reduce their release into the environment. This has included calls for increased monitoring and reporting of PFAS, as well as efforts to develop technologies for the removal of PFAS from wastewater. It is estimated that the annual cost to eliminate PFAS from the environment at the same rate as its current production and usage is equivalent to the entire current global GDP of 106 trillion USD [12]. This has prompted investigation of alternative technologies for the treatment of PFAS-contaminated water. Physical separation processes such as carbon adsorption, membrane filtration, and ion exchange, can remove PFAS from water, however they transfer and concentrate the PFAS from one phase to another instead of degrading them [13, 14]. In contrast, several advanced oxidation methods such as photocatalysis, sonochemical oxidation, and ozonation have reported the successful defluorination and degradation of various PFAS using highly reactive oxygen species (ROS) [15].

3

Amongst these, piezocatalysis, a well-established field, has been extensively investigated for the degradation of organic pollutants in water. In this approach, piezoelectric materials experience an external strain, typically induced by mechanical forces such as ultrasound irradiation to generate ROS. Several piezoelectric materials such as $BaTiO_3$, $BiFeO_3$, ZnO, and $Bi_4Ti_3O_{12}$ with distinct size and morphology have demonstrated their effectiveness in degrading a wide range of organic pollutants [16-23]. Additionally, piezocatalysis can be combined with photocatalysis to overcome the challenges of low light penetration and charge recombination. Furthermore, in the realm of renewable energy sources, mechanical energy emerges as a versatile option, as it can be harnessed from various sources such as water flow, bubbling, and vibrations.

Recent research has shown that piezocatalysis for PFOA degradation could be conducted in the solid phase [24, 25]. Our contribution aims to broaden this research by specifically focusing on PFOS decomposition in the liquid phase. Our objective is to evaluate the potential degradation and defluorination of PFOS in water using $BaTiO_3$ piezocatalytic nanoparticles under ultrasound irradiation (**Figure 1**).
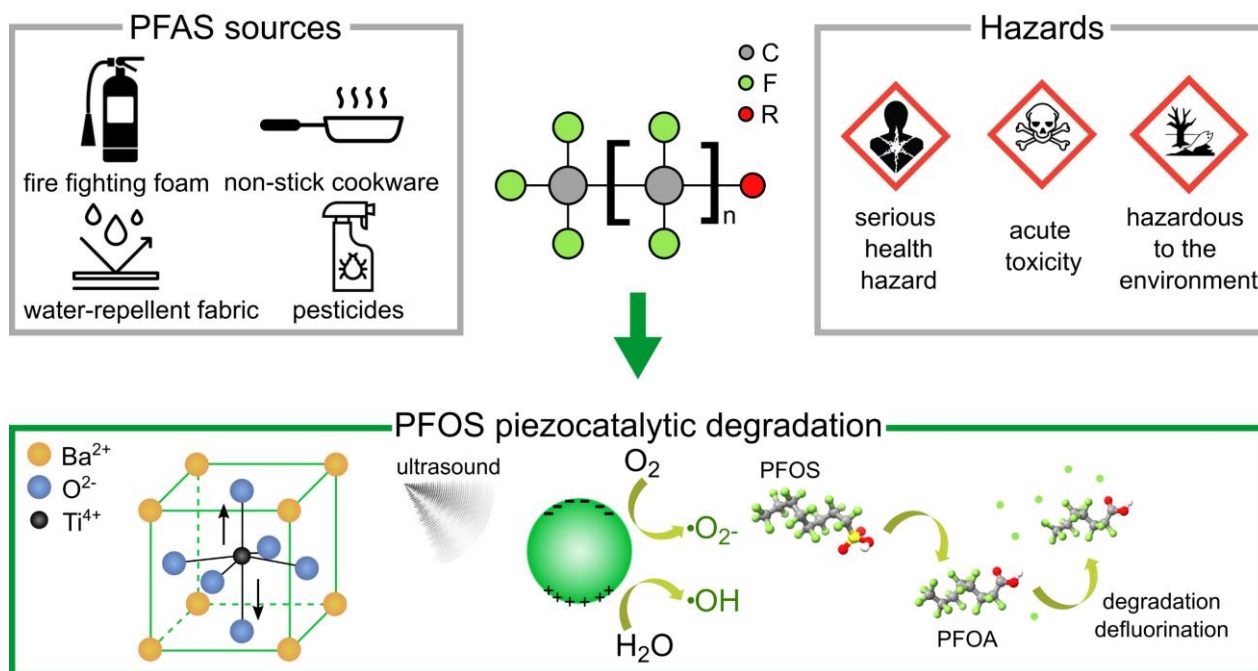

Figure 1. Illustration depicting common sources of PFAS alongside corresponding hazards, and a schematic diagram illustrating the piezocatalytic degradation of PFOS.

2. Results and Discussion

2.1 Material Characterization

Barium titanate (BTO) nanoparticles were synthesized using a two-step hydrothermal method [17]. After the first step, a distinctive nanowire morphology of the $H_2Ti_3O_7$ precursor is

4

observed, as shown in the SEM image in **Figure S4**. Subsequently, after the second hydrothermal step, the formation of BTO nanoparticles with an approximate size of 200 nm was achieved (**Figure 2A**). As seen in **Figure 2B**, EDX mapping was employed to validate the particles composition, confirming the presence of Ba, Ti, and O. Furthermore, to confirm the piezoelectric properties, the nanoparticles' crystal structure was verified by XRD, revealing a pure perovskite structure with characteristic diffraction peaks in agreement with JCPDS No. 81-2203 (**Figure 2C**). The peak splitting of the (002) and (200) planes at $2\theta \sim 45°$ further confirms that the nanoparticles display a tetragonal phase, which confirms the ferroelectric nature of BTO (see **Figure S5**). The formation of the tetragonal phase was further supported by Raman spectroscopy, presented in **Figure 2D**, depicting sharp peaks at 305, 515, and 715 cm^{-1} [26]. Additional insights into the purity of BTO nanoparticles were obtained through XPS analysis. The full XPS spectrum revealed the presence of Ba, Ti, and O elements, as illustrated in **Figure S6**. High-resolution spectra of Ba 3d revealed two split peaks: Ba 3d5/2 at 778 eV and Ba 3d3/2 at 793.4 eV, corresponding to Ba^{2+} (refer to Figure S6b) [27, 28]. Similarly, the Ti 2p spectra exhibited two distinct peaks at 457.5 and 463.3 eV, representing Ti 2p$_{3/2}$ and Ti 2p$_{1/2}$ of Ti^{4+} (see Figure S6c) [29]. Furthermore, the O 1s spectrum displayed a broad peak at
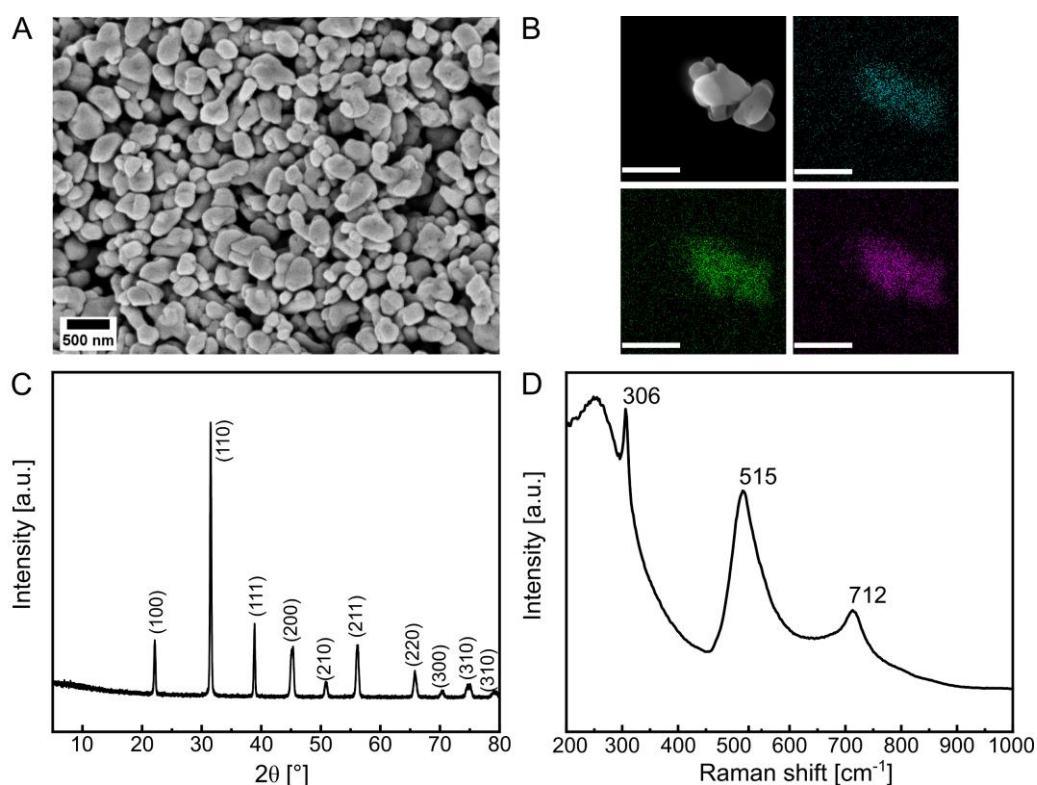
528.8 eV, attributed to lattice oxygen and surface-absorbed oxygen (Figure S6d) [27].

Figure 2. (a) An SEM image of BTO nanoparticles, (b) EDX analysis with elemental mapping revealing barium (green), titanium (purple), and oxygen (blue) (scale = 500 nm). (c) XRD pattern of BTO nanoparticles showcasting the crystal structure. (d) Raman spectra providing insights into the formation of the piezoelectric tetragonal phase.

5

2.2 Piezocatalytic Degradation of PFOS

The BTO nanoparticles, tailored for their piezoelectric properties, were subject to ultrasonic irradiation to induce deformation and external strain. This activation step leverages the piezoelectric characteristics of BTO nanoparticles. By doing so, it facilitates their role as catalysts, generating an electrical potential on the surface of the nanoparticles that serves as a trigger to generate ROS. Consequently, this process leads to the degradation of organic micropollutants, such as PFOS, present in water. For the sake of clarity, note that one must differentiate between mineralization, degradation, and defluorination of PFAS in the context of our study. Degradation involves the transformation of PFAS molecules into other compounds, regardless of defluorination [30]. Mineralization refers to the complete defluorination, irrespective of whether the carbon is fully oxidized [31]. While defluorination specifically refers to the release of inorganic fluorine atoms from PFAS molecules, mineralization does not necessarily occur.

To ensure the efficiency of the piezocatalytic process, initial optimization studies were conducted to determine the optimal catalyst dosage and ultrasound power. As depicted in **Figure S7**, this optimization revealed that the optimal catalyst dosage was found to be 1 mg mL^{-1}. In agreement with previous research, the results indicate that increasing the concentration of the catalyst beyond 1 mg mL^{-1} does not necessarily contribute to a further enhancement of the reaction [32]. Moreover, the ultrasound power stands out as a critical parameter in piezocatalysis, playing a pivotal role in enhancing the decomposition efficiency. However, a tradeoff exists between achieving faster degradation and ensuring that no unintended sonocatalysis is involved in the process [33]. This balance is particularly evident in **Figure S8**, where it is observed that employing 100% of the total power resulted in a gradual decrease of PFOS concentration over time for the control group without the catalyst. Conversely, at 75% power, as illustrated in **Figure 3A** (dashed lines), no significant degradation occurred in the absence of the catalyst. To provide a clear understanding of the individual effects of piezocatalysis, a 75% ultrasound power was selected for the PFOS degradation experiments.

Remarkably, as depicted in Figure 3A, following six hours of ultrasound treatment, the PFOS concentration exhibited a substantial reduction from the initial 4 mg L^{-1} to 0.38 mg L^{-1}, attaining 90.5% removal. As seen in Figure 3B, the extracted ion chromatogram of PFOS at a retention time of 7.55 minutes clearly illustrates a notable difference in peak intensity before and after treatment. In addition, the corresponding degradation kinetics fitted well with the pseudo-first order model (described in SI), revealing a degradation rate of k = 0.06 min^{-1}

6

(**Figure S9**). Note that the initial concentration is notably high, considering that PFOS is typically detected in water at concentrations ranging from nanograms per liter to micrograms per liter [34]. However, an initial large concentration was deliberately selected to facilitate analytical methods for detecting degradation products listed in **Figure 3C**. Nevertheless, as demonstrated in **Figure S10**, this technique is also effective in decomposing PFOS at an order of magnitude lower concentration (0.4 mg L^{-1}), by achieving a 72% PFOS removal.

2.3 Quantification of degradation products

To further corroborate the defluorination of PFOS via piezocatalysis, the fluoride (F$^-$) concentration was monitored over time via ion chromatography, as depicted in **Figure 3D**. Considering that 17 moles of F$^-$ should theoretically be released for each mole of PFOS, the defluorination of $\sim 90\%$ of PFOS after six hours of treatment should generate 2.32 mg L^{-1} of F$^-$. However, 0.74 mg L^{-1} of F$^-$ ions were produced, resulting in an overall defluorination rate of 29%, calculated using **Equation S1**. Regarding the decomposition of PFOS, note that the defluorination ratio is considerably lower compared to the PFOS degradation ratio. This suggests that the transformation of PFOS does not result in complete mineralization. Therefore, preventing secondary pollution arising from the formation of shorter intermediate chains during treatment remains critical. Consequently, the quantification of the degradation products not only ensures a comprehensive understanding of the degradation mechanism but also serves as a crucial step in preventing unintended environmental consequences. PFOS and PFOA stand out as the most frequently detected PFAS in diverse environmental settings, with PFOS consisting of an eight-carbon chain and a sulfonic acid functional group [35]. **Figure 3F** illustrates the concentration increase of PFOA during treatment, suggesting that the initial decomposition step involves the cleavage of the sulfonate end group. This observation aligns with the lower bond energy of the sulfonate end of the PFOS molecule compared to the C-F or C-C bonds, making direct defluorination via nucleophilic substitution much more challenging. Moreover, considering that the C-S bond has a lower bond energy than the C-C bond, and there is a greater distance between the C and S atoms, C-S scission becomes a more favorable pathway [36]. Importantly, the absence of shorter chain perfluoroalkyl sulfonic acids during the screening of degradation products corroborates the desulfonation process.

After four hours of treatment, a subsequent decrease in PFOA concentration is observed indicating a stepwise chain-shortening degradation pathway. As presented in **Figure 3E**, the extracted ion chromatograms after 6 hours of treatment depict a clear formation of shorter-chain perfluorinated carboxylic acids (PFCAs), with primary intermediates identified as perfluoroheptanoic acid (PFHpA, C7), perfluorohexanoic acid (PFHxA, C6),

7

perfluoropentanoic acid (PFPeA, C5), and perfluorobutanoic acid (PFBA, C4). Notably, no fluorotelomer carboxylic acids (FTCAs) were detected during MS screening, ruling out the possibility of a degradation pathway involving H/F exchange. As seen in **Figure 3G**, while the observed trend in the concentration of intermediate products shows a reduction after four hours of treatment, it is essential to highlight that the concentration of these products is three orders of magnitude lower than that of the parent PFOS. The absence of shorter-chain PFCAs in the initial PFOS solution suggests that all detected compounds result from the piezocatalytic degradation. Nonetheless, it is important to note that the total mass balance of the reaction remains incomplete.

The fluorine mass balance is composed of organic fluorine from the detected degradation products and remaining parent compound, free F^- ions, and unidentified fluorine compounds. Free inorganic fluoride was measured directly, whereas the organic fluorine found in the liquid phase was estimated using the final concentrations of PFOS and the identified products. Of the total fluorine that was initially present, the remaining PFOS and degradation products accounted for 10% at the end of the treatment, plus the 29% free F^-. The unaccounted 61% may originate from volatile organofluorine compounds mostly in the gas phase, and possible F^- sorbed on the surface of the BTO nanoparticles, as further discussed in **Section 2.5**.
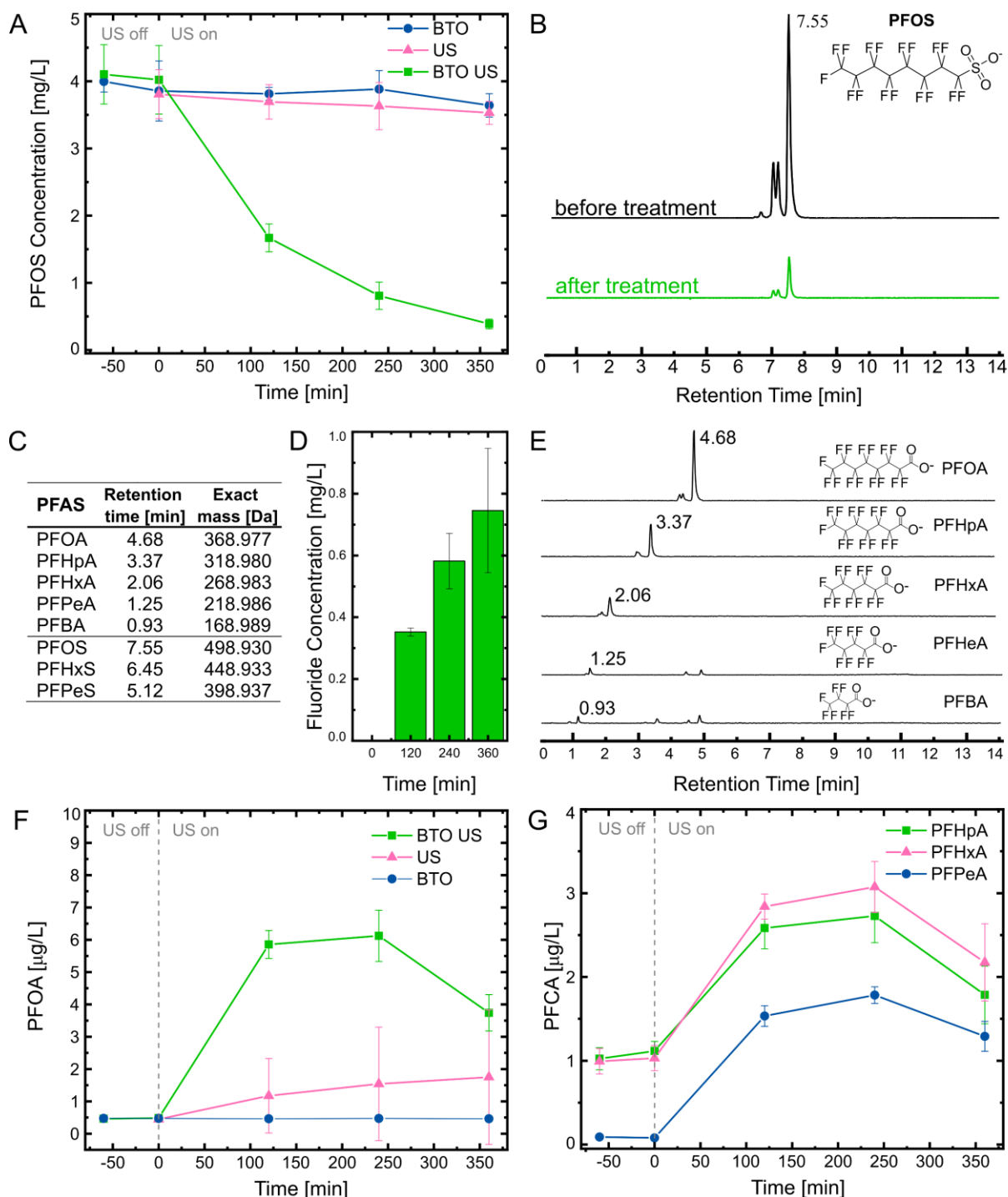
Figure 3. (a) Time course of PFOS piezocatalytic degradation in the presence of BTO nanoparticles, and controls. (b) Extracted ion chromatogram of PFOS before and after treatment. (c) Retention time and exact mass of deprotonated PFOS and PFCAs (the latter detected as decarboxylated ions). (d) Fluoride concentration over treatment time. (e) Extracted ion chromatograms of the detected degradation products after six hours of treatment representing the depicted corresponding carboxylate species. (f) Time course of PFOA production (and later decomposition) under US in the presence of BTO nanoparticles, and (g) time course of shorter chain intermediates PFHpA (C7), PFHxA (C6), PFPeA (C5).

9

2.4 PFOS Removal Mechanism

Piezoelectric materials, such as BTO, exhibit a non-centro-symmetrical crystal structure. As a consequence, under mechanical deformation, the piezomaterial becomes electrically polarized. The polarization induced by mechanical stress triggers the separation of holes (h^+) and electrons (e^-). Hence, a potential difference exists across the material (**Equation 1**). The magnitude of this piezoelectric potential is crucial, as it must meet or exceed the redox potential required for the desired chemical reaction to occur [37]. As illustrated in **Equation 2** and **3**, the free electrons oxidize water to produce hydroxyl radicals ($\cdot OH$), while holes reduce dissolved O_2 to generate superoxide radicals ($O_2^{\cdot-}$). While both radicals are considered predominant active species for the degradation of organic pollutants, $O_2^{\cdot-}$ may indirectly contribute to the degradation by serving as a crucial source for $\cdot OH$ formation rather than directly participating in the degradation process. The formation of $\cdot OH$ is found to follow two pathways: the reaction of holes with water (Equation 2) and the two-electron reduction of $\cdot O_2^-$ as described in **Equations 4** and **5**.

$$BaTiO_3 + US \rightarrow BaTiO_3 \ (e^- + h^+) \tag{1}$$

$$h^+ + H_2O \rightarrow \cdot OH + H^+ \tag{2}$$

$$O_2 + e_{aq}^- \rightarrow \cdot O_2^- \tag{3}$$

$$\cdot O_2^- + e_{aq}^- + 2H^+ \rightarrow H_2O_2 \tag{4}$$

$$H_2O_2 \rightarrow \cdot OH + \cdot OH \tag{5}$$

Previous studies have shown that BTO piezocatalysts can generate both reactive species, where the concentration of generated $\cdot OH$ is observed to be significantly higher than that of $\cdot O_2^-$ [16]. To examine the main reactive species involved in the PFOS degradation, the piezocatalytic reaction was assessed in the presence of scavenging agents. Tert-Butyl alcohol (TBA), ethylenedinitrilotetraacetic acid disodium salt dihydrate (EDTA), and L-ascorbic acid (LAA) were used as common scavengers to quench $\cdot OH$, H^+, and $\cdot O_2^-$, respectively [38, 39]. As seen in **Figure 4A**, the results show a significant decrease in degradation efficiency after adding TBA, emphasizing the crucial role of $\cdot OH$. The inhibiting effect was less pronounced with LAA, suggesting an auxiliary role of $\cdot O_2^-$. Moreover, the degradation efficiency showed a decrease, albeit not complete suppression, after adding EDTA, indicating that the formation of $\cdot OH$ partly originates from H^+ and $\cdot O_2^-$.

As seen in **Figure 4B-D**, in the presence of TBA and EDTA, there is a minimal generation of PFOA and PFCAs, confirming that PFOS is not being decomposed in the absence of $\cdot OH$ and H^+. Intriguingly, when LAA is introduced, the production of shorter-chain PFCAs surpasses that observed without scavengers. Unlike the scenario without scavengers, where the

10

concentration of degradation products begins to decrease during treatment, the presence of LAA leads to a saturation point after two hours.
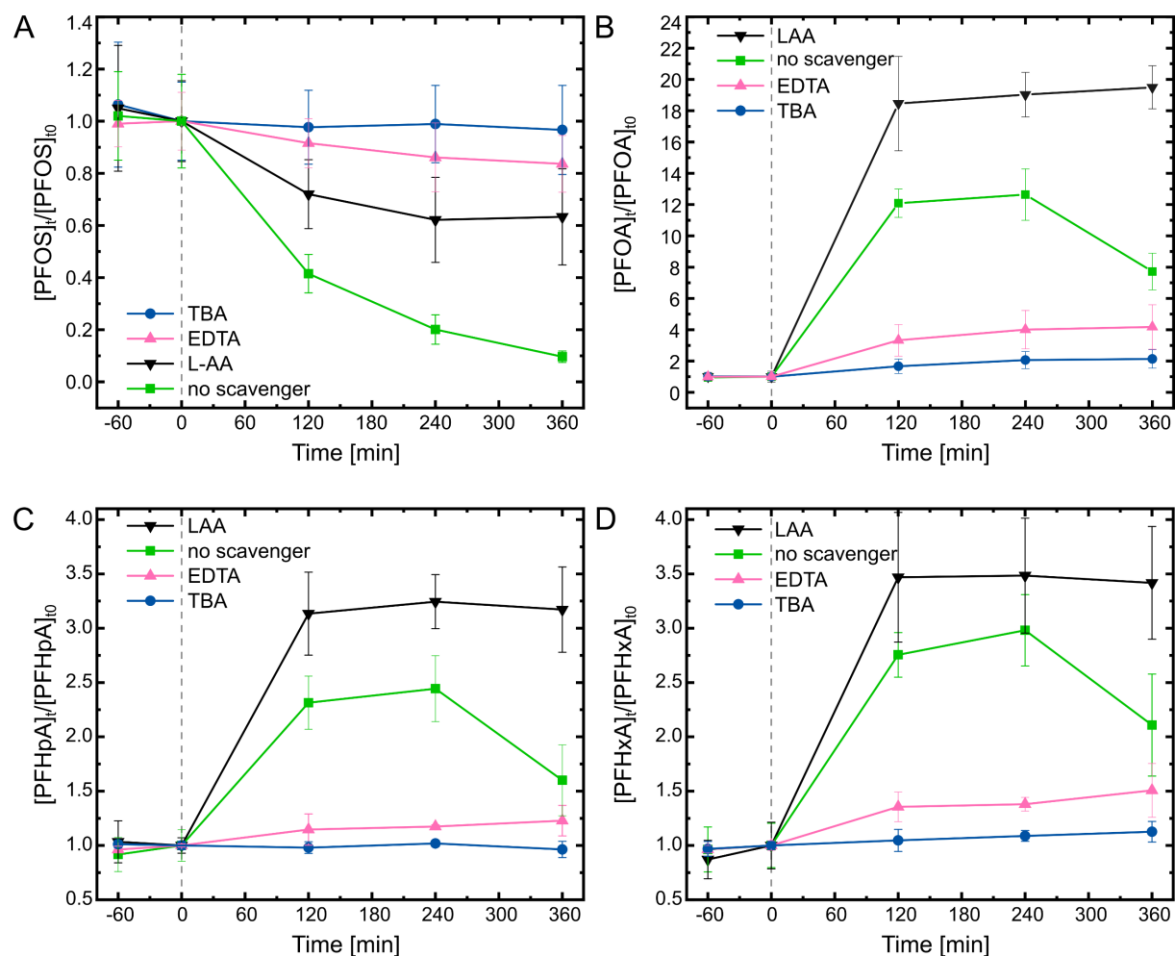

Figure 4. (a) Piezocatalytic decomposition of PFOS in the presence of scavenging agents TBA, EDTA, and LAA, trapping •OH, h^+, and •O_2^-, respectively. Time course of detected shorter chain intermediates: (b) PFOA (C8), (c) PFHpA (C7), and (d) PFHxA (C6).

2.5 Practical Implications

To assess the performance over extended use of the BTO nanoparticles, three piezocatalytic degradation cycles of PFOS were conducted, where ultrasound activation was extended to 12 and 18 hours. After each cycle, the nanoparticles were collected via centrifugation and dispersed in a fresh 4 mg L^{-1} PFOS solution. As depicted in **Figure 5A**, the final concentrations achieved after each cycle were recorded as 0.5, 1.4, and 2.1 mg L^{-1}. Notably, the rate constant for PFOS exhibited a significant decrease in the second and third cycles, resulting in an overall reduction in degradation of approximately 54%. The addition of nanoparticles into a fresh PFOS solution in each cycle eliminated the possibility of smaller chain products accumulating and causing a decrease in performance. Consequently, further investigation was pursued by collecting the BTO nanoparticles to examine the potential saturation of their surface with adsorbed PFOS or PFCAs. For this purpose, XPS measurements were conducted (**Figure S11**).

11

The only visible difference in spectra between the nanoparticles before and after treatment was the presence of a peak at F 1s. As seen in **Figure 5B**, no peak is visible before treatment however, after treatment, a distinct peak centering at 685 eV emerges. Given that no peaks were identified visible around 688 eV, which commonly indicates the presence of the C-F bond, this peak was ascribed to the negatively charged fluoride ions [40]. In this regard, the adsorbed F^- also contributes to the incomplete mass balance discussed above. In addition, it is speculated that surface passivation competitively inhibits adsorption of the target PFAS, thereby reducing interactions with the generated ROS.

In the realm of water treatment, it is crucial to assess real-world conditions where water often contains various inorganic ions and organic matter constituents. To investigate the practical applicability of piezocatalysis in degrading PFOS, experiments were conducted using lake water from Rotsee, Switzerland, and wastewater treatment plant effluent (WWTP) from Palapye, Botswana, both spiked with PFOS at a concentration of 4 mg L^{-1} using 1 g L^{-1} of BTO nanoparticles. The characteristics of lake water and sewage effluent are outlined in **Table S3**. In comparison to deionized water, both lake water and sewage effluent showed reduced removal efficiencies, likely due to the presence of natural organic matter and suspended solids acting as scavengers for ROS, thus impeding the degradation of target contaminants [41]. Despite these challenges, as depicted in **Figure S12**, PFOS degradation in lake water and WWTP effluent reached approximately 30% and 50%, respectively, highlighting its potential application in natural water matrices. Nevertheless, transitioning from laboratory-scale studies with controlled conditions to real-world scenarios necessitates careful consideration of the water matrix composition and its impact on treatment processes. Additional investigations should be conducted to examine the specific impact of inorganic cations and anions found in natural waters.
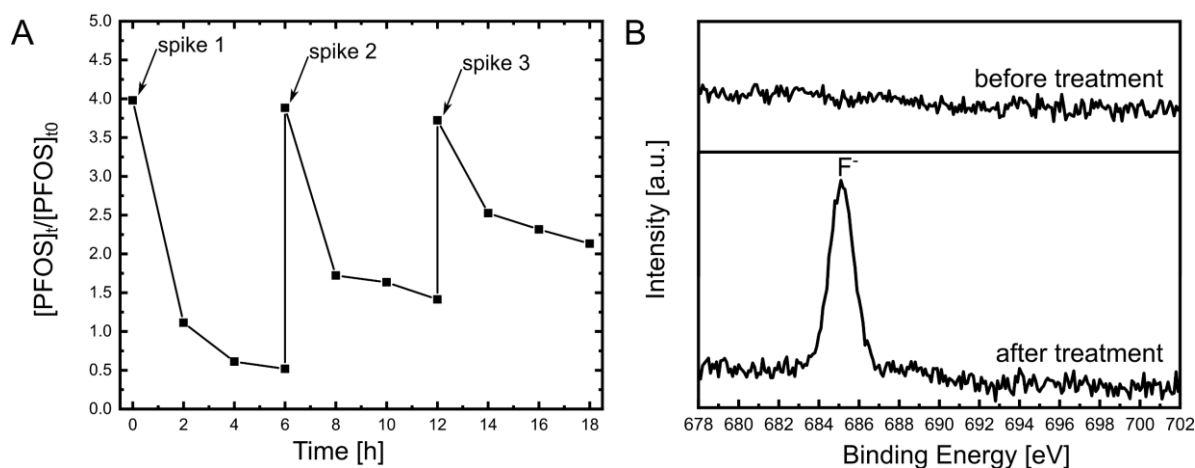
12

Figure 5. (a) Time-dependent decomposition profile with PFOS spikes to evaluate the reusability of BTO nanoparticles. (b) F 1s XPS spectra of BTO nanoparticles before and after treatment.

3. Conclusion

Our study addresses the urgent need for effective water treatment strategies to combat the environmental and health hazards posed by PFAS. Through piezocatalysis using BTO nanoparticles under ultrasound irradiation, we successfully achieved substantial degradation of PFOS in water, attaining a remarkable 90.5% removal after six hours of treatment. Furthermore, the quantification of degradation products provided valuable insights into the transformation pathways of PFOS, shedding light on the formation and further degradation of shorter-chain PFCAs. Continued research in this field is crucial to further validate the efficacy of piezocatalytic technologies for real-world applications, paving the way for sustainable solutions to PFAS contamination challenges. Further investigation of alternative piezoelectric materials, novel mechanical activation sources, and synergistic combinations with sonocatalysis or piezocatalysis holds promise for optimizing the efficiency of the piezocatalytic degradation process aimed at PFAS removal.

13

4. Materials and Methods

Chemicals, materials, and data analysis are presented in the Supporting Information.

4.1 BaTiO$_3$ Nanoparticle Synthesis

To manufacture BaTiO$_3$ nanoparticles, we first produced precursor H$_2$Ti$_3$O$_7$ nanowires by mixing 0.7987 g of TiO$_2$ with 35 mL of 10 M NaOH solution. The mixture was then transferred into an autoclave and heated for 24 hours at 240 °C. The resulting nanowires were washed three times with water and 0.2 M hydrochloric acid solution (HCl) and soaked for 6-12 hours in HCl with the same concentration. The nanowires were then washed again with deionized (DI) water until reaching a pH of 7, followed by drying at 80 °C. In the second hydrothermal step, barium was introduced to form the nanoparticles. 35 mL of degassed DI water was prepared by bubbling with N$_2$ for 10 minutes. Then, 2.208 g of Ba(OH)$_2$·8H$_2$O were added, and the mixture was stirred and sonicated until complete dispersion. Next, 0.2576 g of H$_2$Ti$_3$O$_7$ precursor was added and dispersed in the mixture. The resulting suspension was transferred into an autoclave and heated to 240 °C for 12 hours. The synthesized BTO nanoparticles were washed with a 0.2 M HCl solution and DI water, followed by drying at 80 °C.

4.2 Material Characterization

Scanning electron microscopy (SEM) was performed using a Zeiss ULTRA 55 instrument equipped with an energy dispersive X-ray spectroscopy (EDX) detector to determine the elemental composition of the samples. The samples were drop-casted onto a silicon wafer and coated with a thin layer of palladium and gold to ensure conductivity before SEM analysis. Images were taken at 5 eV, with a 30 aperture and 10 mm working distance.

Raman inVia Renishaw confocal microscope using a 514 nm excitation wavelength. The spectral acquisition conditions were: objective 50× (NA = 0.75), wavelength 514 nm, laser power 4.8 mW, exposure time 2 s, and 5 accumulations using a grating with 1800 grooves per millimeter.

X-ray diffraction (XRD) measurements were performed on an Empyrean diffractometer with a copper X-ray source (λ = 1.5406 Å) and a PIXcel detector (Malvern Panalytical). The dispersion of nanoparticles in ethanol was drop-casted onto a silicon wafer and let to air dry.

X-ray photoelectron spectroscopy (XPS) experiments were performed in ESFOSCAN at CCiTUB, an equipment based on the PHI 5000 VersaProbe 4 instrument from Physical Electronics (ULVAC-PHI). The measurements have been done with a monochromatic focused X-ray source (Aluminium Kα line of 1486.6 eV) calibrated using the 3d$_{5/2}$ line of Ag with a full width at half maximum (FWHM) of 0.6 eV. The analyzed area was a circle of 100 µm of diameter, samples placed at 45° with respect to the analyzer axis, and the selected resolution

14

for the spectra was 224 eV of Pass Energy and 0.8 eV/step for the general spectra, and 27 eV of Pass Energy and 0.1 eV/step for the high-resolution spectra of the selected elements. A combination of low energy electron and ion (Ar$^+$) guns (both less than 5 eV) was used to discharge samples if necessary. Measurements are referenced to the C 1s signal, whose binding energy is equal to 284.8 eV in adventitious carbon (from atmospheric contamination). Measurements were made in an ultra-high vacuum (UHV) chamber at a pressure between 5E^{-10} and 5E^{-9} Torr.

4.3 Piezocatalysis Degradation Experiments

A 50 mL PFOS solution (4 mg L^{-1}) was used for all degradation experiments with a 1 mg mL^{-1} BTO nanoparticle concentration. The ultrasonic treatment was administered using the Sonocool 255 (Bandelin) ultrasonic bath, operating at a frequency of 35 kHz, while maintaining a constant temperature of 24 °C and applying a power of 135 W (75% of total power). Before each experiment the ultrasound was degassed for 10 minutes. The 100 mL glass beaker was always placed in the center position, covered, and held in place with a rack (see **Figure S1**). To achieve the desired 4 mg L^{-1} concentration, the PFOS solution was prepared by diluting a stock solution of 3200 ppm. This dilution was accomplished by adding 1.25 mL of the PFOS stock solution to 1 L of deionized water. The resulting solution was stirred overnight prior to separation into 50 mL glass vials and subsequently frozen. Before each experiment, the vials were thawed at room temperature. Subsequently, the nanoparticles were added and stirred for an additional 30 minutes in darkness to attain absorption-desorption equilibrium. All degradation experiments were conducted over a total time span of 6 hours, during which 1 mL aliquots were collected every two hours. To ensure the separation of the nanoparticles, the collected aliquots underwent two rounds of centrifugation at 14,000 rpm, separated, before being stored in the freezer for subsequent analysis. Control experiments were conducted to confirm that no degradation occurred in the absence of nanoparticles or ultrasound. Prior to initiating the experiments, PFOS adsorption on the nanoparticles was quantified by stirring the dispersion in dark for 60 min and time aliquots were taken before and after for analysis. In addition, a 4 mg L^{-1} PFOS solution without nanoparticles was also exposed to six hours of ultrasound vibrations.

For the scavenger experiments, after thawing the prepared PFOS solution, 0.1 mM of tert-Butyl alcohol (TBA) (pH = 5.66), ethylenedinitrilotetraacetic acid disodium salt dihydrate (EDTA) (pH = 4.80), or L-ascorbic acid (LAA) (pH = 3.45), were mixed in before the addition of the BTO nanoparticles.

15

For the cycling experiments, at the end of the 6 hour treatment the BTO dispersion in PFOS solution was centrifuged at 11,000 rpm for 30 minutes and the isolated pellet was left to dry in the oven at 60 °C overnight. The catalyst was weighed and re-used with a new 4 mg L^{-1} PFOS solution.

To investigate the decomposition of PFOS, the concentration of the initial product and its degradation products as well as the fluoride ions were determined using a Waters Acquity ultra-performance liquid chromatography (UPLC) system coupled with tandem mass spectrometry (MS) and an ion chromatography system (881 Compact IC pro), respectively. All analytical methods and data analysis are described in Text S2.

16

Acknowledgements

17

References

1.	Ackerman Grunfeld, D.; Gilbert, D.; Hou, J.; Jones, A. M.; Lee, M. J.; Kibbey, T. C. G.; O'Carroll, D. M., Underestimated burden of per- and polyfluoroalkyl substances in global surface waters and groundwaters. *Nature Geoscience* **2024,** *17* (4), 340-346, 10.1038/s41561-024-01402-8.

2.	Begley, T. H.; White, K.; Honigfort, P.; Twaroski, M. L.; Neches, R.; Walker, R. A., Perfluorochemicals: Potential sources of and migration from food packaging. *Food Addit Contam A* **2005,** *22* (10), 1023-1031, 10.1080/02652030500183474.

3.	Baduel, C.; Paxman, C. J.; Mueller, J. F., Perfluoroalkyl substances in a firefighting training ground (FTG), distribution and potential future release. *Journal of Hazardous Materials* **2015,** *296*, 46-53, 10.1016/j.jhazmat.2015.03.007.

4.	Lallas, P. L., The Stockholm Convention on persistent organic pollutants. *Am J Int Law* **2001,** *95* (3), 692-708, 10.2307/2668517.

5.	Zareitalabad, P.; Siemens, J.; Hamer, M.; Amelung, W., Perfluorooctanoic acid (PFOA) and perfluorooctanesulfonic acid (PFOS) in surface waters, sediments, soils and wastewater - A review on concentrations and distribution coefficients. *Chemosphere* **2013,** *91* (6), 725-732, 10.1016/j.chemosphere.2013.02.024.

6.	Kannan, K.; Corsolini, S.; Falandysz, J.; Fillmann, G.; Kumar, K. S.; Loganathan, B. G.; Mohd, M. A.; Olivero, J.; Van Wouwe, N.; Yang, J. H.; Aldous, K. M., Perfluorooctanesulfonate and related fluorochemicals in human blood from several countries. *Environmental Science & Technology* **2004,** *38* (17), 4489-4495, 10.1021/es0493446.

7.	Monroy, R.; Morrison, K.; Teo, K.; Atkinson, S.; Kubwabo, C.; Stewart, B.; Foster, W. G., Serum levels of perfluoroalkyl compounds in human maternal and umbilical cord blood samples. *Environmental Research* **2008,** *108* (1), 56-62, 10.1016/j.envres.2008.06.001.

8.	Reinhardt, M.; Kozel, R.; Zimmermann, S.; Rupp, H.; Zoller, O.; Hoehn, E., Perfluorinated chemicals in Swiss groundwater - results of the National Groundwater Monitoring NAQUA. *Iahs-Aish P* **2011,** *342*, 112-+,

9.	Barry, V.; Winquist, A.; Steenland, K., Perfluorooctanoic Acid (PFOA) Exposures and Incident Cancers among Adults Living Near a Chemical Plant. *Environ Health Persp* **2013,** *121* (11-12), 1313-1318, 10.1289/ehp.1306615.

10.	Ingelido, A. M.; Marra, V.; Abballe, A.; Valentini, S.; Iacovella, N.; Barbieri, P.; Porpora, M. G.; Di Domenico, A.; De Felip, E., Perfluorooctanesulfonate and perfluorooctanoic acid exposures of the Italian general population. *Chemosphere* **2010,** *80* (10), 1125-1130, 10.1016/j.chemosphere.2010.06.025.

11.	Crawford, N. M.; Fenton, S. E.; Strynar, M.; Hines, E. P.; Pritchard, D. A.; Steiner, A. Z., Effects of perfluorinated chemicals on thyroid function, markers of ovarian reserve, and natural fertility. *Reprod Toxicol* **2017,** *69*, 53-59, 10.1016/j.reprotox.2017.01.006.

12.	Ling, A. L., Estimated scale of costs to remove PFAS from the environment at current emission rates. *Science of the Total Environment* **2024,** *918*, 170647 10.1016/j.scitotenv.2024.170647.

13.	Smaili, H.; Ng, C., Adsorption as a remediation technology for short-chain per- and polyfluoroalkyl substances (PFAS) from water - a critical review. *Environ Sci-Wat Res* **2023,** *9* (2), 344-362, 10.1039/d2ew00721e.

14.	Das, S.; Ronen, A., A Review on Removal and Destruction of Per- and Polyfluoroalkyl Substances (PFAS) by Novel Membranes. *Membranes-Basel* **2022,** *12* (7), 10.3390/membranes12070662.

15.	Mojiri, A.; Zhou, J. L.; Ozaki, N.; KarimiDermani, B.; Razmi, E.; Kasmuri, N., Occurrence of per- and polyfluoroalkyl substances in aquatic environments and their removal by advanced oxidation processes. *Chemosphere* **2023,** *330*, 138666 10.1016/j.chemosphere.2023.138666.

16.   Tang, Q.; Wu, J.; Kim, D.; Franco, C.; Terzopoulou, A.; Veciana, A.; Puigmartí-Luis, J.; Chen, X. Z.; Nelson, B. J.; Pané, S., Enhanced Piezocatalytic Performance of BaTiO3 Nanosheets with Highly Exposed {001} Facets. *Adv Funct Mater* **2022,** *32* (35), 2202180 10.1002/adfm.202202180.

17.   Wu, J.; Xu, Q.; Lin, E. Z.; Yuan, B. W.; Qin, N.; Thatikonda, S. K.; Bao, D. H., Insights into the Role of Ferroelectric Polarization in Piezocatalysis of Nanocrystalline BaTiO. *Acs Appl Mater Inter* **2018,** *10* (21), 17842-17849, 10.1021/acsami.8b01991.

18.   Masekela, D.; Hintsho-Mbita, N. C.; Sam, S.; Yusuf, T. L.; Mabuba, N., Application of BaTiO3-based catalysts for piezocatalytic, photocatalytic and piezo- photocatalytic degradation of organic pollutants and bacterial disinfection in wastewater: A comprehensive review. *Arab J Chem* **2023,** *16* (2), 104473 10.1016/j.arabjc.2022.104473.

19.   Mushtaq, F.; Chen, X. Z.; Hoop, M.; Torlakcik, H.; Pellicer, E.; Sort, J.; Gattinoni, C.; Nelson, B. J.; Pané, S., Piezoelectrically Enhanced Photocatalysis with BiFeO3 Nanostructures for Efficient Water Remediation. *Iscience* **2018,** *4*, 236-+, 10.1016/j.isci.2018.06.003.

20.   Xu, X. L.; Jia, Y. M.; Xiao, L. B.; Wu, Z., Strong vibration-catalysis of ZnO nanorods for dye wastewater decolorization via piezo-electro-chemical coupling. *Chemosphere* **2018,** *193*, 1143-1148, 10.1016/j.chemosphere.2017.11.116.

21.   Ning, X. E.; Hao, A. Z.; Cao, Y. L.; Hu, J. D.; Xie, J.; Jia, D. Z., Effective promoting piezocatalytic property of zinc oxide for degradation of organic pollutants and insight into piezocatalytic mechanism. *J Colloid Interf Sci* **2020,** *577*, 290-299, 10.1016/j.jcis.2020.05.082.

22.   Bai, Y.; Zhao, J. Z.; Lv, Z. L.; Lu, K., Enhanced piezocatalytic performance of ZnO nanosheet microspheres by enriching the surface oxygen vacancies. *J Mater Sci* **2020,** *55* (29), 14112-14124, 10.1007/s10853-020-05053-z.

23.   Tang, Q.; Wu, J.; Chen, X. Z.; Sanchis-Gual, R.; Veciana, A.; Franco, C.; Kim, D.; Surin, I.; Pérez-Ramfrez, J.; Mattera, M.; Terzopoulou, A.; Qin, N.; Vukomanovic, M.; Nelson, B. J.; Puigmartf-Luis, J.; Pan, S., Tuning oxygen vacancies in Bi4Ti3O12 nanosheets to boost piezo-photocatalytic activity. *Nano Energy* **2023,** *108*, 10.1016/j.nanoen.2023.108202.

24.   Guo, R. N.; Li, L.; Zhao, Z. W.; Zhang, S., Enhanced piezoelectric catalysis of BaTiO3 by ZVAl for mechanochemical defluorination of PFOA: Promotion of electron transfer. *Journal of Hazardous Materials* **2024,** *465*, 10.1016/j.jhazmat.2023.133040.

25.   Yang, N. Y.; Yang, S. S.; Ma, Q. Q.; Beltran, C.; Guan, Y. Q.; Morsey, M.; Brown, E.; Fernando, S.; Holsen, T. M.; Zhang, W.; Yang, Y., Solvent-Free Nonthermal Destruction of PFAS Chemicals and PFAS in Sediment by Piezoelectric Ball Milling. *Environmental Science & Technology* **2023**, 10.1021/acs.estlett.2c00902.

26.   Deng, Z.; Dai, Y.; Chen, W.; Pei, X. M.; Liao, J. H., Synthesis and Characterization of Bowl-Like Single-Crystalline BaTiO3 Nanoparticles. *Nanoscale Res Lett* **2010,** *5* (7), 1217-1221, 10.1007/s11671-010-9629-7.

27.   Wang, R. X.; Zhu, Q.; Wang, W. S.; Fan, C. M.; Xu, A. W., BaTiO-graphene nanocomposites: synthesis and visible light photocatalytic activity. *New J Chem* **2015,** *39* (6), 4407-4413, 10.1039/c4nj02272f.

28.   Ma, Y. P.; Luo, H.; Zhou, X. F.; Guo, R.; Dang, F.; Zhou, K. C.; Zhang, D., Suppressed polarization by epitaxial growth of SrTiO on BaTiO nanoparticles for high discharged energy density and efficiency nanocomposites. *Nanoscale* **2020,** *12* (15), 8230-8236, 10.1039/c9nr08572f.

29.   Guan, G. G.; Gao, G. J.; Xiang, J.; Yang, J. N.; Gong, L.; Chen, X.; Zhang, Y. M.; Zhang, K. Y.; Meng, X. F., CoFe/BaTiO Hybrid Nanofibers for Microwave Absorption. *Acs Appl Nano Mater* **2020,** *3* (8), 8424-8437, 10.1021/acsanm.0c01855.

30.   Smith, S. J.; Lauria, M.; Higgins, C. P.; Pennell, K. D.; Blotevogel, J.; Arp, H. P. H., The Need to Include a Fluorine Mass Balance in the Development of Effective Technologies

for PFAS Destruction. *Environmental Science & Technology* **2024,** *58* (6), 2587-2590, 10.1021/acs.est.3c10617.

31.   Horst, J.; McDonough, J.; Ross, I.; Houtz, E., Understanding and Managing the Potential By-Products of PFAS Destruction. *Ground Water Monit R* **2020,** *40* (2), 17-27, 10.1111/gwmr.12372.

32.   Prasanna, G.; Nguyen, H. D. P.; Dunn, S.; Karunakaran, A.; Marken, F.; Bowen, C. R.; Le, B. N. T.; Nguyen, H. D.; Pham, T. P. T., Impact of stirring regime on piezocatalytic dye degradation using BaTiO3 nanoparticles. *Nano Energy* **2023,** *116*, 10.1016/j.nanoen.2023.108794.

33.   Bössl, F.; Tudela, I., Piezocatalysis: Can catalysts really dance? *Curr Opin Green Sust* **2021,** *32*, 10.1016/j.cogsc.2021.100537.

34.   Evich, M. G.; Davis, M. J. B.; McCord, J. P.; Acrey, B.; Awkerman, J. A.; Knappe, D. R. U.; Lindstrom, A. B.; Speth, T. F.; Tebes-Stevens, C.; Strynar, M. J.; Wang, Z.; Weber, E. J.; Henderson, W. M.; Washington, J. W., Per- and polyfluoroalkyl substances in the environment. *Science* **2022,** *375* (6580), eabg9065, 10.1126/science.abg9065.

35.   Teymourian, T.; Teymoorian, T.; Kowsari, E.; Ramakrishna, S., A review of emerging PFAS contaminants: sources, fate, health risks, and a comprehensive assortment of recent sorbents for PFAS treatment by evaluating their mechanism. *Research on Chemical Intermediates* **2021,** *47* (12), 4879-4914, 10.1007/s11164-021-04603-7.

36.   Deng, Y.; Liang, Z. H.; Lu, X. W.; Chen, D.; Li, Z.; Wang, F., The degradation mechanisms of perfluorooctanoic acid (PFOA) and perfluorooctane sulfonic acid (PFOS) by different chemical methods: A critical review. *Chemosphere* **2021,** *283*, 10.1016/j.chemosphere.2021.131168.

37.   Starr, M. B.; Wang, X. D., Fundamental Analysis of Piezocatalysis Process on the Surfaces of Strained Piezoelectric Materials. *Sci Rep-Uk* **2013,** *3*, 10.1038/srep02160.

38.   Duan, L.; Wang, B.; Heck, K.; Guo, S.; Clark, C. A.; Arredondo, J.; Wang, M.; Senftle, T. P.; Westerhoff, P.; Wen, X.; Song, Y.; Wong, M. S., Efficient Photocatalytic PFOA Degradation over Boron Nitride. *Environmental Science & Technology Letters* **2020,** *7* (8), 613-619, 10.1021/acs.estlett.0c00434.

39.   Song, Z.; Dong, X. L.; Wang, N.; Zhu, L. H.; Luo, Z. H.; Fang, J. D.; Xiong, C. H., Efficient photocatalytic defluorination of perfluorooctanoic acid over BiOCl nanosheets via a hole direct oxidation mechanism. *Chemical Engineering Journal* **2017,** *317*, 925-934, 10.1016/j.cej.2017.02.126.

40.   Zhang, K. L.; Huang, J.; Yu, G.; Zhang, Q. W.; Deng, S. B.; Wang, B., Destruction of Perfluorooctane Sulfonate (PFOS) and Perfluorooctanoic Acid (PFOA) by Ball Milling. *Environmental Science & Technology* **2013,** *47* (12), 6471-6477, 10.1021/es400346n.

41.   Wang, J. L.; Wang, S. Z., Effect of inorganic anions on the performance of advanced oxidation processes for degradation of organic contaminants. *Chemical Engineering Journal* **2021,** *411*, 10.1016/j.cej.2020.128392.